

PAPER • OPEN ACCESS

Temporal statistics of residual wavefront variance of an adaptive optics system

To cite this article: Jian Huang *et al* 2019 *J. Opt.* **21** 125606

View the [article online](#) for updates and enhancements.



IOP | ebooks™

Bringing together innovative digital publishing with leading authors from the global scientific community.

Start exploring the collection—download the first chapter of every title for free.

Temporal statistics of residual wavefront variance of an adaptive optics system

Jian Huang^{1,2} , Hong Zhou^{3,4}, Jinsheng Yang^{3,4}, Chao Liu^{3,4} and Hao Xian^{3,4}

¹University of Electronic Science and Technology of China, School of Astronautics & Aeronautics, Chengdu, 611731, People's Republic of China

²State Key Laboratory of Applied Optics, Changchun Institute of Optics, Fine Mechanics and Physics, China Academy of Sciences, Changchun, 130033, People's Republic of China

³The Key Laboratory on Adaptive Optics, Chinese Academy of Sciences, Chengdu 610209, People's Republic of China

⁴Institute of Optics and Electronics, Chinese Academy of Sciences, Chengdu 610209, People's Republic of China

E-mail: huangjian81@uestc.edu.cn

Received 3 July 2019, revised 12 October 2019

Accepted for publication 30 October 2019

Published 21 November 2019



CrossMark

Abstract

We present the probability density function (PDF) for the residual wavefront variance of an adaptive optics system that includes control error, the fitting error of a deformable mirror, and Hartmann sensor detecting noise. The PDF is directly connected to adaptive optics system parameters and the spatiotemporal strength parameters of atmospheric turbulence, and it can be described as a generalized Chi square distribution. Our results provide a more precise theory for adaptive optics systems compared to the current theory based on the ensemble average. Thus, this study can contribute to the development of high-resolution and high-stability adaptive optics systems for astronomy and optical communications in the atmosphere.

Keywords: adaptive optics, residual wavefront variance, probability method

(Some figures may appear in colour only in the online journal)

1. Introduction

Adaptive optics (AO) systems are widely applied in astronomical imaging and atmospheric optical communications because of their ability to correct wavefront aberrations [1–6]. The current theory for AO systems is based on the ensemble average, and it provides the relationship between system parameters and average residual wavefront variance. Tyson and Hardy [7, 8] presented most of the ensemble equations for AO systems in their books. The effectiveness of ensemble equations relies on a single fact: if we design an AO system with a mean wavefront variance of 1 rad^2 , 50% of images probably have a quality better than 1 rad . Moreover, there is a

certain probability ($\sim 10^{-4}$) of obtaining excellent images with a Strehl ratio of 0.9. However, the exact probability for the distribution of wavefront variance or image quality can never be determined using only current ensemble average results.

A Strehl ratio of over 0.9 is required for the AO systems used in large telescopes for extrasolar planet observations [9, 10]. However, building an AO system with an average Strehl ratio of 0.9 that uses visible wavelength, as expected in next-generation AO (NGAO) systems, is a technical challenge [11]. Lucky imaging may be required for AO; this would require research on how 'lucky' an AO system is. The current ensemble equations of AO cannot provide the temporal variation information of wavefront spatial variance, which makes the stability and accuracy required by NGAO difficult to analyze [11].

The stability of an AO system becomes extremely important when it is applied in optical communications



Original content from this work may be used under the terms of the [Creative Commons Attribution 3.0 licence](https://creativecommons.org/licenses/by/3.0/). Any further distribution of this work must maintain attribution to the author(s) and the title of the work, journal citation and DOI.

through the atmosphere. Optical communications systems require high availability or stability. A given data package cannot be discarded as in astronomical imaging. If the AO characteristics for imaging and communications are compared, the 1000th-qualified (for a given threshold) AO wavefront compensation for imaging may be acceptable for a quasi-static astronomical object. In contrast, such a performance would mean an unacceptable bit error rate of 10^{-3} for an optical communications link. Therefore, an AO system for imaging can have low availability, but an AO system for optical communications must have extremely high stability.

Generally, the large difference in information bandwidths for imaging and communications requires different analysis methods for AO systems in different scenarios. The frequency of astronomical imaging has a magnitude of 1 Hz. The closed-loop bandwidth of an AO system is hundreds of hertz, and the bit rate for optical communications can be in gigahertz. Imaging quality is approximately the average of hundreds of frames with AO compensation. Thus, the ensemble method is applicable to AO design. On the contrary, millions of signal bits are contained in one sample interval of AO compensation. Hence, communications performance can only be precisely calculated with the probability distribution of the AO compensation metric, which has a nonlinear correlation with the bit error rate [12].

In 2008, Gladysz *et al* investigated the temporal variability and statistics for the instantaneous Strehl ratio of AO compensation and presented a three-parameter gamma distribution model for AO wavefront variance [13], which they used to discuss the distribution of the Strehl ratio. Canales and Cagigal investigated the speckle statistics of partially compensated AO system [14, 15]. Their works gave the patterns of the AO correction performance indexes such as phase variance, Strehl ratio and received speckle on image plane. However, the relationship between the distribution model and AO system parameters in the form of equations has not been reported yet. In 2016, we presented the probability density function (PDF) of an AO system as a function of the closed-loop bandwidth and atmospheric Greenwood frequency [16]. In this study, we integrate control error, fitting error, and Hartmann sensor detecting error to produce a comprehensive PDF equation for an AO system with determined parameters.

The principle of this work is based on a linear system description of an AO system, where the Zernike coefficients of a reconstructed wavefront are a linear combination of subaperture centroid vectors from different error sources. We can analyze the probability distribution of wavefront error from the randomness of the centroid errors corresponding to residual wavefront error.

2. Hartmann sensor detecting error

The typical structure of an AO system is shown in figure 1. A wavefront aberration is sensed by a Hartmann sensor. A wavefront controller controls a tilt mirror (TM) and a

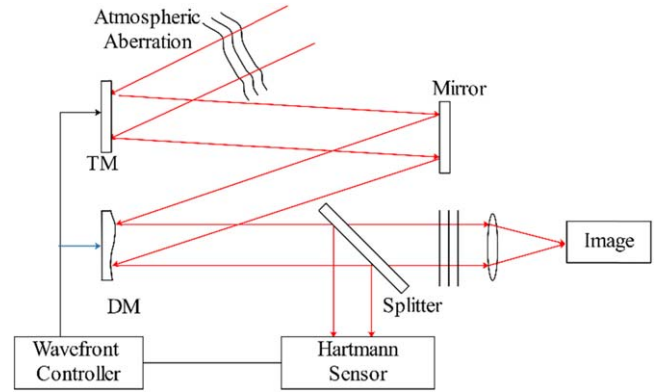


Figure 1. Structure of a typical AO system.

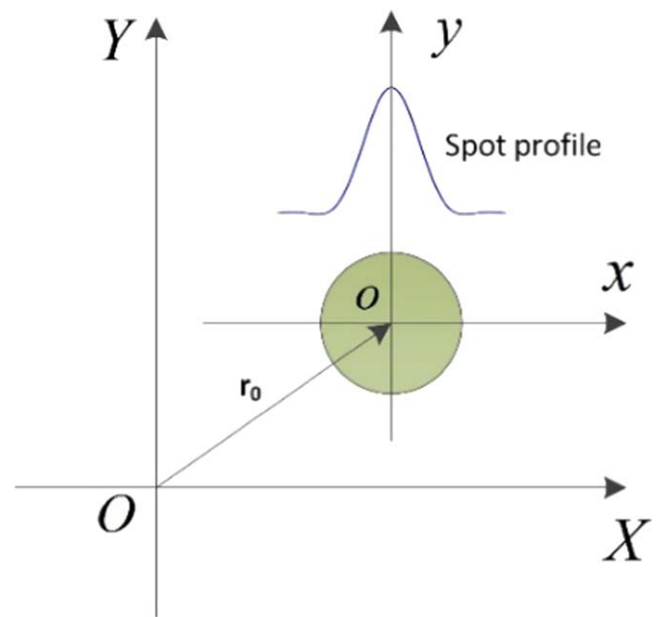


Figure 2. Coordinate definition for the subaperture of a Hartmann sensor.

deformable mirror (DM) to correct atmospheric tilt and high-order aberration separately in real time. The four main components constitute the independent TM and DM closed-loops, and the residual wavefront error of the AO system is mainly determined by the error factors in these four components.

In general, only two main types of noise are analyzed in the Hartmann sensor detecting error: photon shot noise and readout noise [17]. We can neglect high-order aberrations and assume that only tilt exists on the subapertures of the Hartmann sensor when the AO is in a closed loop. Thus, all spots on the subapertures have an ideal Airy profile with different center shifts. As shown in figure 2, the coordinate on a subaperture is OXY after the Hartmann sensor is calibrated. The other coordinate, oxy , is located at the center of the exact Airy spot. Hence, \mathbf{r}_0 denotes the centroid shift on the subaperture. Here, we only calculate the x value of centroid error. The centroid error on the y axis is statically identical to that on the

x axis. Therefore, the centroid error due to detecting error can be calculated from the sums on all X coordinates as

$$\begin{aligned} \Delta x &= \frac{\sum K \cdot X}{\sum K} - \frac{\sum K_0 \cdot X}{\sum K_0} \\ &= \frac{\sum [(K - K_0)X]}{\sum K} - \frac{\sum (K - K_0)}{\sum K} \cdot \frac{\sum (K_0 \cdot X)}{\sum K_0}, \end{aligned} \quad (1)$$

where K denotes the received photon count at coordinate X , K_0 denotes the corresponding photon count without noise, and $K - K_0$ is the photon fluctuation caused by noise. If we define the spot centroid without noise as X_0 , then

$$\frac{\sum (K_0 \cdot X)}{\sum K_0} = X_0. \quad (2)$$

If the X coordinate is expressed as $X = X_0 + x$, where the zero point of the x coordinate is the centroid of the spot, then equation (1) can be rewritten as

$$\begin{aligned} \Delta x &= \frac{\sum [(K - K_0)(X_0 + x)]}{\sum K} - \frac{\sum (K - K_0)}{\sum K} \cdot \frac{\sum (K_0 \cdot X)}{\sum K_0} \\ &= \frac{\sum (K - K_0)}{\sum K} X_0 + \frac{\sum [(K - K_0)x]}{\sum K} - \frac{\sum (K - K_0)}{\sum K} X_0 \\ &= \frac{\sum (K - K_0)x}{\sum K}. \end{aligned} \quad (3)$$

Clearly, the centroid error due to the Hartmann sensor is determined by the signal-to-noise ratio and spatial distribution of noise.

Here, we want to focus the effect of noise, therefore, only tilts on Hartmann subaperture are considered by assuming the Hartmann sensor has adequate spatial sampling frequency. Otherwise, the sampling error of Hartmann subapertures should be included.

2.1. Photon shot noise

For photon shot noise, the received photon count, K , is randomly distributed as a Poisson distribution with expectation $E(K) = K_0$ and variance $D(K) = K_0$. The expectation of the photon count on the subaperture is centrosymmetric because it is proportional to the intensity profile of the spot. Therefore, we can calculate the centroid error caused by shot noise in polar coordinates, as shown in figure 3. Then, we can express centroid error as

$$\Delta x = \frac{\sum_r r \sum_\theta (K - K_0) \cos \theta}{\sum_r \sum_\theta K}, \quad (4)$$

and

$$K_0 = \frac{I(r)}{hvF} r dr d\theta, \quad (5)$$

where I is intensity, hv is photon energy, F is the frame frequency of the Hartmann camera, $I(r)$ is the intensity

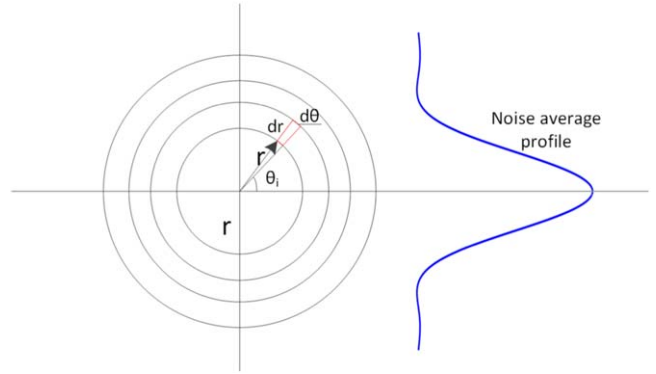


Figure 3. Photon count profile in polar coordinates.

function of the Airy spot, and

$$I(r) = I_0 \left[\frac{2J_1(\pi d_l r / \lambda f)}{\pi d_l r / \lambda f} \right]^2, \quad (6)$$

where I_0 is the peak intensity, λ is the wavelength, f and d_l are the focal length and diameter, respectively, of the microlens of the Hartmann sensor, and $J_1(\cdot)$ is the first-order Bessel function of the first kind.

For each subaperture, the denominator in equation (4) is the total photon count in one frame image. It follows the Poisson distribution, and its average is

$$\begin{aligned} V &= E \left(\sum_r \sum_\theta K \right) = \sum_r \sum_\theta K_0 = \int \int_{-\infty}^{\infty} \frac{I(r)}{hvF} r dr d\theta \\ &= \frac{4I_0}{hvF} \int_0^{2\pi} \int_0^{\infty} \left(\frac{J_1(\pi d_l r / \lambda f)}{\pi d_l r / \lambda f} \right)^2 r dr d\theta \\ &= \frac{4I_0}{\pi hvF} \left(\frac{\lambda f}{d_l} \right)^2. \end{aligned} \quad (7)$$

To calculate the value of the numerator in equation (4), we consider the random variable series in the inner part of the sum $\{(K - K_0)_i \cos \theta_i\}$, where subscript i denotes area i ($r dr d\theta$) at polar coordinates (r, θ_i) . Clearly, random variable series $P_i = (K - K_0)_i \cos \theta_i$ are independent of each other, but they have different PDF functions and a corresponding expectation, $\mu_i = E(P_i) = 0$, and variance, $\sigma_i^2 = D(P_i) = \cos^2(\theta_i) K_0$.

If we define

$$\begin{aligned} s_n^2 &= \sum_{i=1}^{\infty} \sigma_i^2 = K_0 \sum_{i=1}^{\infty} \cos^2(\theta_i) \\ &= \frac{I(r)}{hvF} r dr \int_0^{2\pi} \cos^2(\theta) d\theta = \frac{\pi I(r)}{hvF} r dr, \end{aligned} \quad (8)$$

then

$$\begin{aligned} &\lim_{k \rightarrow \infty} \frac{1}{s_n^{2+p}} \sum_{i=1}^k E[|\cos(\theta_i) K_i - \cos(\theta_i) K_0|^{2+p}] \\ &= \lim_{k \rightarrow \infty} \sum_{i=1}^k \frac{E[|\cos(\theta_i) K_i - \cos(\theta_i) K_0|^{2+p}]}{s_n^{2+p}} \\ &\stackrel{|\cos(\theta) \leq 1|}{\leq} \lim_{k \rightarrow \infty} \sum_{i=1}^k E \left[\left(\frac{|K_i - K_0|}{s_n} \right)^{2+p} \right]. \end{aligned} \quad (9)$$

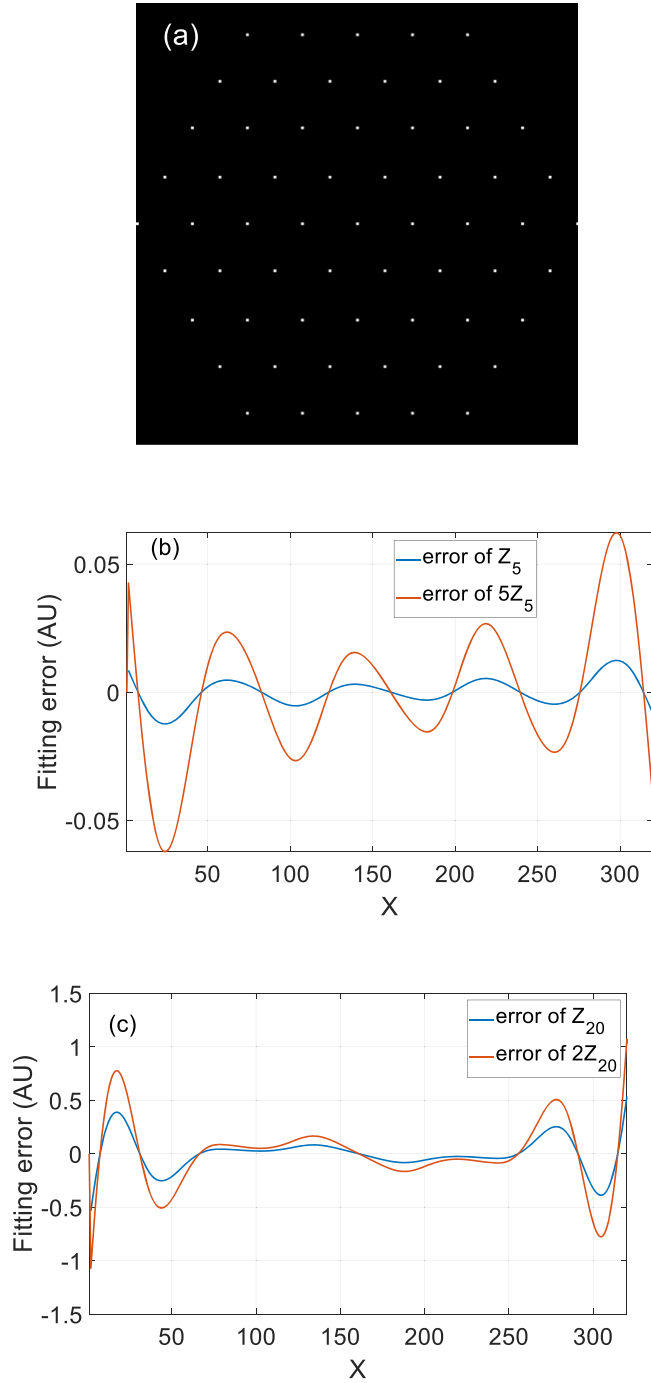


Figure 4. Simulation of the fitting error: (a) configuration of the 61-cell deformable mirror, (b) fitting errors of Z_5 and $5Z_5$ on the X axis, and (c) fitting errors of Z_{20} and $2Z_{20}$ on the x axis.

In equation (9), $d\theta = 2\pi/k \rightarrow 0$ when $k \rightarrow \infty$. Then, $|K_i - K_0| < s_n$ is always satisfied when ring width $dr > 0$. Thus, the limit of equation (9) is zero when positive integer p approaches infinity. Therefore, according to the Lyapunov condition of the central limit theorem, the sum of the inner term of the numerator in equation (4), i.e. $\sum_{\theta} (K - K_0) \cos \theta$, is a Gaussian random variable, and the value of the numerator

in equation (4) is the linear combination of Gaussian random variables, $N(0, s_n^2)$. Consequently, the value of the numerator in equation (4) follows a Gaussian distribution with zero mean and variance:

$$\sigma_u^2 = \sum_r r^2 s_n^2 = \sum_r r^2 \frac{\pi I(r)}{hvF} r dr. \quad (10)$$

We can calculate equation (10) in the integral form as

$$\begin{aligned} \sigma_u^2 &= \int_0^R r^2 \frac{\pi I(r)}{hvF} r dr = \frac{4\pi I_0}{hvF} \int_0^R r^3 \left[\frac{J_1(\pi d_l r / \lambda f)}{\pi d_l r / \lambda f} \right]^2 dr \\ &\stackrel{\pi d_l r / \lambda f = u}{=} \frac{4\pi I_0}{hvF} \left(\frac{\lambda f}{\pi d_l} \right)^4 \int_0^{\frac{\pi d_l}{\lambda f} R} [J_1(u)]^2 u du \\ &= \frac{V}{\pi^2} \left(\frac{\lambda f}{d_l} \right)^2 \int_0^{\frac{\pi d_l}{\lambda f} R} [J_1(u)]^2 u du. \end{aligned} \quad (11)$$

where R is the radius of the area on the Hartmann sensor corresponding to one subaperture. Considering that equation (11) diverges when $R \rightarrow \infty$, we can set the second dark ring as the integral radius in which most photons of the Airy spot are detected, i.e. $R = 2.233 \lambda f / d_l$. Then, we have

$$\begin{aligned} \sigma_u^2 &= \frac{V}{\pi^2} \left(\frac{\lambda f}{d_l} \right)^2 \int_0^{7.016} [J_1(u)]^2 u du \\ &\approx \frac{2.22V}{\pi^2} \left(\frac{\lambda f}{d_l} \right)^2. \end{aligned} \quad (12)$$

For two independent random variables A and B , the variance $D(A/B)$ approximately equals to $D(A)/E^2(B)$ when $E(A) = 0$ and $D(B) \langle E^2(B) \rangle$ [18]. In equation (4), the numerator obeys Gaussian distribution with zero mean value; the denominator obeys Poisson distribution, its variance and expectation $D(\sum K) = E(\sum K) = V$, and $V \gg 1$ (namely $D(\sum K) \langle E^2(\sum K) \rangle$). Therefore, if the inequality of the total photon count among all subapertures due to scintillation can be neglected, every element in the centroid error vector, \mathbf{z}_{ph} , caused by photon shot noise has the same variance. Its value can be calculated by connecting equations (4), (5), (7), and (12),

$$\sigma_{ph}^2 = \frac{\sigma_u^2}{V^2} = \frac{2.22}{\pi^2 V} \left(\frac{\lambda f}{d_l} \right)^2 \approx \frac{1}{V} \left(0.47 \frac{\lambda f}{d_l} \right)^2. \quad (13)$$

On other side, we have $D(\sum K) = E(\sum K)$ for the total photon count of the subaperture spot on Hartmann sensor, the variation of $\sum K$ is about several $\sqrt{\sum K_0}$, which means $\sum K$ could be approximated as a constant (i.e. $\sum K_0$) for a practical AO system in which the subaperture spots have over hundreds of photons. Therefore, the centroid error Δx in equation (4) approximately obeys Gaussian distribution.

Note that the equivalent Gaussian width of the Airy spot is $\sigma_A = 0.45 \lambda f / d_l$. Hence, equation (13) provides mostly the same results as Cao and Yu [19]. The centroid error variance of photon shot noise is inversely proportional to the total photon count, and it is affected by the parameters for the microlens of the Hartmann sensor according to equation (13).

2.2. Readout noise

The readout noise on Hartmann sensor pixels follows a Gaussian distribution. Thus, the centroid error from readout noise can be calculated according to equation (3):

$$\Delta x = \frac{\sum_{ij} n_{ij} \cdot x_{ij}}{\sum_{ij} (P_{ij} + n_{ij})}, \quad (14)$$

where P_{ij} is the ideal photon count on pixel, n_{ij} is the noise equivalent photon count on pixel ij , and x_{ij} is the coordinate of pixel ij . The numerator in equation (14) is a linear combination of Gaussian random variables. The sum also follows a Gaussian distribution. Moreover, the centroid error caused by readout noise can still be considered as a Gaussian random variable, similar to the analysis of photon shot noise.

Note that the zero point of the coordinate is located at the center of the spot. Thus, the mean value of the numerator in equation (14) is zero, and its variance is [19]

$$\sigma_r^2 = \frac{\sigma_{rd}^2 HL(L^2 - 1)}{12V^2}, \quad (15)$$

where σ_{rd}^2 denotes the readout noise variance at each pixel and L and H are the numbers of pixels in the X and Y directions, respectively. The centroid variance caused by readout noise is inversely proportional to the square of spot power and proportional to readout noise variance.

3. Fitting error

An AO system is typically analyzed as a linear system. The temporal characteristics of the fitting error of a DM can be modeled in the same manner. This implies that (1) the fitting error of a DM is the linear sum of each Zernike mode when mode coupling is neglected, (2) the spatial shape is similar when single modes with different magnitudes are fitted, and (3) the magnitude of fitting error is proportional to the magnitude of the fitted wavefront.

To examine these three assumptions, we modeled a 61-cell DM to fit the Zernike mode, $Z_m(x, y)$. The fitting error for $Z_m(x, y)$ is [20]

$$s_m(x, y) = Z_m(x, y) - \sum_{k=1}^{61} b_k H_k(x, y), \quad (16)$$

where $H_k(x, y)$ indicates actuator influence functions and b_k denotes the related coefficients of actuators. The actuator arrangement used in the simulation is shown in figure 4(a). The white points denote the centers of the actuators. We used this DM to fit the fifth-order and 20th-order Zernike modes, Z_5 and Z_{20} , with different magnitudes. The residual errors on the X axis in arbitrary units (AU) are presented in figures 4(b) and (c). The linear characteristics of the DM can be clearly observed. If the fitting error of Z_5 is $s_5(x, y)$, then the fitting error of $5Z_5$ is equal to $5s_5(x, y)$. The proportionality between the curves is consistent at all points.

The fitting error function, $s_m(x, y)$, for the Zernike mode of order m is determined by the configuration and actuator influence functions of the DM. $s_m(x, y)$ can be measured using an interferometer when the DM is used to fit each Zernike mode. Then, the centroid error vector, \mathbf{c}_m , from $s_m(x, y)$ can be determined when the configurations of the DM and Hartmann subaperture are matched. \mathbf{c}_m comprises the x and y centroid errors caused by $s_m(x, y)$, and it can be expressed as the product of the average slope and focal length of the microlens on each subaperture.

$$\begin{aligned} \mathbf{c}_m &= [c_{m,1}, c_{m,2}, c_{m,3}, c_{m,4}, \dots, c_{m,2N-1}, c_{m,2N}]^T \\ &= f \left[\left\langle \frac{\partial s_m(x, y)}{\partial x} \right\rangle_1, \left\langle \frac{\partial s_m(x, y)}{\partial y} \right\rangle_1, \right. \\ &\quad \times \left. \left\langle \frac{\partial s_m(x, y)}{\partial x} \right\rangle_2, \left\langle \frac{\partial s_m(x, y)}{\partial y} \right\rangle_2, \right. \\ &\quad \dots, \left. \left\langle \frac{\partial s_m(x, y)}{\partial x} \right\rangle_N, \left\langle \frac{\partial s_m(x, y)}{\partial y} \right\rangle_N \right]^T, \quad (17) \end{aligned}$$

Here, N is the number of subapertures of the Hartmann sensor and f is the focal length of the microlens. $\langle \cdot \rangle_n$ represents the spatial average on subaperture n . Here, we assume that the spatial frequency of the Hartmann sensor is unlimited; hence, aliasing error is neglected.

According to Noll's analysis, the Zernike coefficients of Kolmogorov turbulence a_m have a Gaussian distribution with an average of zero [21]. Therefore, the total centroid error vector is the linear combination of all Zernike modes:

$$\mathbf{z}_f = \sum_m a_m \mathbf{c}_m. \quad (18)$$

The variance of a_m is only determined by the radial order, n , of the corresponding Zernike mode:

$$\sigma_{a_m}^2 = \frac{2.246(n+1)\Gamma(n-5)}{[\Gamma(17/6)]^2\Gamma(n+23/6)} \left(\frac{D}{\rho_0} \right)^{5/3}, \quad (19)$$

where $\Gamma(\cdot)$ is the gamma function, D is the telescope diameter, and ρ_0 is the atmosphere coherent length (or Fried constant). We assume that the fluctuations of the Zernike modes are independent. Equations (18) and (19) indicate that the centroid error vector caused by the DM follows a Gaussian distribution. The variance vector corresponding to \mathbf{z}_f is

$$\sigma_{z_f}^2 = \left[\sum_{m=1}^M (\sigma_{a_m}^2 c_{m,1}^2), \sum_{m=1}^M (\sigma_{a_m}^2 c_{m,2}^2), \dots, \sum_{m=1}^M (\sigma_{a_m}^2 c_{m,2N}^2) \right]^T. \quad (20)$$

4. PDF for the residual wavefront variance

The Zernike coefficient vector, \mathbf{A}_r , due to insufficient control bandwidth has a Gaussian distribution [16], and the variance

of each element is

$$\sigma_{t,m}^2 = \begin{cases} 5.75 \left(\frac{f_{TG}}{f_{t-3dB}} \right)^2 & m = 1, 2; \text{ (tilt)} \\ \frac{1}{M-2} \left(\frac{f_G}{f_{d-3dB}} \right)^{5/3} & m = 3, 4, \dots, M; \text{ (high-order)} \end{cases}, \quad (21)$$

where f_{TG} is the tilt Greenwood frequency of atmospheric turbulence, f_{t-3dB} is the tilt-control system bandwidth (3 dB cutoff frequency), f_G is the Greenwood frequency of high-order Zernike aberrations, f_{d-3dB} is the bandwidth of the DM control loop, and M is the Zernike mode number in the wavefront reconstruction.

We can obtain the Zernike coefficient vector by adding control error, detecting error, and fitting error:

$$\mathbf{A} = \mathbf{R} \cdot (\mathbf{z}_{ph} + \mathbf{z}_r + \mathbf{z}_f) + \mathbf{A}_t, \quad (22)$$

where \mathbf{R} is the constant reconstruction matrix of the AO system.

All elements in the vectors on the right side of equation (22) follow a Gaussian distribution. Consequently, as the sum of a linear combination of Gaussian random variables, each element in \mathbf{A} follows a Gaussian distribution with zero mean. Their variances, σ_m^2 , can easily be calculated by utilizing the above equations:

$$\begin{aligned} \sigma_m^2 &= (\sigma_{ph}^2 + \sigma_r^2) \sum_{j=1}^{2N} R_{m,j}^2 + \sigma_{t,m}^2 \\ &+ [R_{m,1}^2, R_{m,2}^2, \dots, R_{m,2N}^2] \cdot \left[\sum_{m=1}^M (\sigma_{a_m}^2 c_{m,1}^2), \right. \\ &\left. \sum_{m=1}^M (\sigma_{a_m}^2 c_{m,2}^2), \dots, \sum_{m=1}^M (\sigma_{a_m}^2 c_{m,2N}^2) \right]^T. \end{aligned} \quad (23)$$

In equation (23), the atmospheric fluctuations of Zernike mode amplitudes are assumed to be approximately independent. Our simulation shows that the effect of the covariance of Zernike coefficients on the PDF of the residual wavefront is negligible. However, a strict expression can be obtained using Karhunen–Loève modes, in which equations (17) and (19) are replaced by the results of the Karhunen–Loève expansion [22, 23].

If we use the standard Zernike polynomials with unit variance, the total residual wavefront (spatial) variance of an AO system is equal to the sum of the squares of the elements of \mathbf{A} :

$$\sigma_{wf}^2 = \mathbf{A}^T \mathbf{A}. \quad (24)$$

According to probability theory, the temporal variation in the residual wavefront (spatial) variance of an AO system follows the generalized χ^2 distribution. Its PDF is extremely complicated, and it could be approximated by a single-gamma distribution with the same mean and variance [24].

We can also rewrite equation (24) in the following form:

$$\sigma_{wf}^2 = \sum_{m=1}^M A_m^2, \quad (25)$$

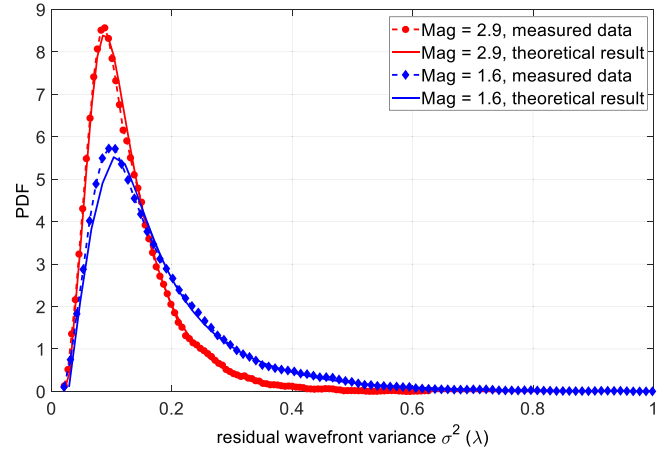


Figure 5. PDFs for the residual wavefront variance obtained from the measured wavefront data and theoretical analysis.

where element $A_m \sim N(0, \sigma_m^2)$. Then, it is easy to determine that A_m^2 follows the gamma distribution, $\text{Gamma}(1/2, 2\sigma_m^2)$. The PDF is given by

$$f(A_m^2) = \frac{\sqrt{2}}{\Gamma(1/2)} (\sigma_m^2 A_m^2)^{-1/2} \exp\left(-\frac{A_m^2}{2\sigma_m^2}\right), \quad (26)$$

where $\Gamma(\cdot)$ is the gamma function. The PDF of σ_{wf}^2 can be obtained by the consecutive convolution of all $f(A_m^2)$. After the PDF of the wavefront variance of an AO system is obtained, the index of availability (or stability) could be calculated by the integral of the PDF of wavefront variance from zero to a given upper boundary, as discussed in our previous work [16].

We examined the PDF equations using the residual wavefront data of an AO system for a 1.8 m diameter telescope operated by the Adaptive Optics Laboratory of the Chinese Academy of Science [25, 26]. This AO system consists of two closed loops to independently control its TMs and DMs with 127 actuators using a proportional integral controller. The Hartmann sensor runs at $0.55 \mu\text{m}$ with an image acquisition frequency of 2000 Hz. The data were measured for two stars with magnitudes of 2.9 and 1.6, and the corresponding atmospheric coherent lengths were 7.9 cm and 9.3 cm at $0.55 \mu\text{m}$, respectively. Each measurement consisted of 10 000 frames of wavefront data acquired in 5 s.

The wavefront data were reconstructed from the first 35 Zernike polynomials. We found that the histogram of every Zernike coefficient strongly agreed with the Gaussian function with different variances. The PDFs of residual wavefront variance were calculated using the wavefront data and theoretical equations. The results are shown in figure 5.

As shown in figure 5, the theoretical analysis of the PDF of residual wavefront variance agrees well with the closed-loop AO system data. Comparing the PDF curves between $\text{Mag} = 2.9$ and $\text{Mag} = 1.6$, their residual high-order aberrations are almost the same. The difference mainly arises from different tilt correction performances, which show a large tail on the right of the PDF curve. The large tail would considerably degrade long exposure image quality and receiving

efficiency in optical communication. Therefore, the primary object of AO optimization is to eliminate the tail of the PDF curve of wavefront variance. In other words, we should improve the tilt correction ability of an AO system first by increasing the control bandwidth of the TM, as discussed in [14]. Then, we would expect the PDF curve to shift to the centrosymmetric shape along with decrease in residual tilt. This issue could be analyzed from the point of view of the skewness of the PDF curve.

The skewness of the PDF curve of AO residual wavefront variance can also be theoretically estimated from its PDF equations. The skewness of $f(A_m^2)$ is

$$\gamma_m = E \left[\left(\frac{A_m^2 - \mu_m}{\sqrt{2}\sigma_m^2} \right)^3 \right] = 2\sqrt{2}, \quad (27)$$

where μ_m is the expectation of A_m^2 and σ_m is the root mean square of A_m^2 , as given in equation (23). Then, the skewness of residual wavefront variance is

$$\begin{aligned} \gamma_{wfs} &= E \left[\left(\frac{\sigma_{wfs}^2 - \mu_{\sigma_{wfs}^2}}{\sigma_{\sigma_{wfs}^2}} \right)^3 \right] = E \left[\left(\frac{\sum_{m=1}^M A_m^2 - \sum_{m=1}^M \mu_m}{\sqrt{\sum_{m=1}^M \sigma_m^4}} \right)^3 \right] \\ &= \frac{1}{\left(\sum_{m=1}^M 2\sigma_m^4\right)^{3/2}} E \left[\left(\sum_{m=1}^M A_m^2 - \sum_{m=1}^M \mu_m \right)^3 \right] \\ &= \frac{1}{\left(\sum_{m=1}^M 2\sigma_m^4\right)^{3/2}} \sum_{m=1}^M E[(A_m^2 - \mu_m)^3]. \end{aligned} \quad (28)$$

Substituting equation (27) into (28) gives

$$\gamma_{wfs} = 2\sqrt{2} \frac{\sum_{m=1}^M (\sqrt{2}\sigma_m^2)^3}{\left(\sum_{m=1}^M 2\sigma_m^4\right)^{3/2}} = \frac{2\sqrt{2}\sum_{m=1}^M \sigma_m^6}{\left(\sum_{m=1}^M \sigma_m^4\right)^{3/2}}. \quad (29)$$

According to equation (29), the PDF of residual wavefront variance σ_{wf}^2 is always positively skewed. The skewness values according to the experimental data and equation (29) are 1.70 and 1.78, respectively, for the curves of $M = 2.9$, and 2.02 and 2.32, respectively, for the curves of $M = 1.6$.

If residual tilt can be neglected for a fine tilt correction loop, residual higher-order Zernike terms dominate the residual wavefront, and σ_m^2 is almost the same for higher-order terms, then the skewness of the PDF of residual wavefront variance σ_{wf}^2 is approximated by

$$\gamma_{wfs} \approx \frac{2\sqrt{2}}{\sqrt{M}}. \quad (30)$$

The PDF curve of residual wavefront variance approaches centrosymmetry for large M . However, because of the negative exponential calculation from wavefront variance to the Strehl ratio, the PDF of the Strehl ratio may have negative skewness for a small average of σ_{wf}^2 . The negative skewness converts to positive skewness as the average of σ_{wf}^2 increases, as shown by Gladysz *et al* [13].

5. Discussion and conclusions

In this work, we obtained the Gaussian characteristics of Zernike coefficients of AO residual wavefront from the randomness of error sources. Furthermore, we obtained the connection between the distribution model and AO structure parameters, which made it possible to predict the distribution model at the beginning of system design.

The AO theory is mainly constructed according to the ensemble average, which is used to estimate average AO system performance and for system design in the past. Through the linear system analysis for an AO system, we developed a group of equations that connected the PDF of AO residual wavefront variance with AO system parameters and turbulence parameters. These equations could directly guide AO design and optimization with higher precision. Moreover, the PDF was a complete mathematical description for a random process. Therefore, the results in this paper provide a helpful framework for investigating the principle of AO systems from the viewpoint of probability for all AO applications.

In future, more error sources, such as aliasing error, discrete sampling error, and isoplanatic error, must be considered for furthering investigating the probability characteristics of the random process of AO compensation. Certain other topics are also important, such as the errors due to non-integral controllers and non-Hartmann sensing in AO systems. Moreover, the boundary conditions for each type of error should be clarified for different AO application scenarios and specific configuration of AO system. This will help to balance the error budget and optimize system performance, and finally to construct the complete probability theory of the AO system.

Acknowledgments

The authors thank Professors Xinyang Li and Wenhan Jiang for the helpful discussions. The work is supported by National Natural Science Foundation of China (NSFC) (61405023, 61501097); Funds of the Adaptive Optics Laboratory, CAS (LAOF201501).

ORCID iDs

Jian Huang  <https://orcid.org/0000-0003-2314-7104>

References

- [1] Sodnik Z, Armengol J, Czichy R and Meyer R 2009 *Proc. SPIE* **7464** 746406
- [2] Berkefeld T, Soltau D, Czichy R, Fischer E, Wandernoth B and Sodnik Z 2010 *Proc. SPIE* **7736** 77364C
- [3] Kasper M 2012 *Proc. SPIE* **8447** 84470B
- [4] Rao C *et al* 2015 *Chin. Opt. Lett.* **13** 120101

- [5] Canuet L, Védrenne N, Conan J-M, Petit C, Artaud G, Rissons A and Lacan J 2018 *J. Opt. Soc. Am. A* **35** 148
- [6] Chen M, Rui D and Xian H 2018 *Opt. Express* **26** 4230
- [7] Hardy J 1998 *Adaptive Optics for Astronomical Telescope* (Oxford: Oxford University Press)
- [8] Tyson R 2010 *Principles of Adaptive Optics* 3rd edn (Boca Raton, FL: CRC Press)
- [9] Macintosh B et al 2006 *Proc. SPIE* **6272** 62720N
- [10] Jovanovic N et al 2015 *Publ. Astron. Soc. Pac.* **127** 890
- [11] Wizinowich P et al 2008 *Proc. SPIE* **7015** 701511
- [12] Horwath J, David F, Knapek M and Perlot N 2005 *Proc. SPIE* **5712** 1–11
- [13] Gladysz C, Christou J C, Bradford W and Roberts L C 2008 *Publ. Astron. Soc. Pac.* **120** 1132
- [14] Canales V and Cagigal M 1999 *Appl. Opt.* **38** 766
- [15] Cagigal M and Canales V 1998 *Opt. Lett.* **23** 1072
- [16] Huang J, Liu C, Deng K, Yao Z, Xian H and Li X 2016 *Opt. Express* **24** 2818
- [17] Jiang W, Xian H and Shen F 1997 *Proc. SPIE* **3126** 534
- [18] Frishman F 1975 *A Modern Course on Statistical Distributions in Scientific Work* vol 1 (Boston, MA: D. Reidel) pp 401–6
- [19] Cao G and Yu X 1994 *Opt. Eng.* **33** 2333
- [20] Gavel D and Norton A 2014 *Proc. SPIE* **9148** 91484J
- [21] Noll R 1976 *J. Opt. Soc. Am.* **66** 207
- [22] Wang J and Markey J 1978 *J. Opt. Soc. Am.* **68** 78
- [23] Fried D 1966 *J. Opt. Soc. Am.* **56** 1372
- [24] Covo S and Elalouf A 2014 *Electron. J. Statist.* **8** 894
- [25] Rao C et al 2010 *Proc. SPIE* **7654** 76541H
- [26] Wei K et al 2010 *Chin. Opt. Lett.* **8** 1019